Recovery of Salinity Gradient Energy with an Inorganic Sodium Superionic Conductor

Guodong Zhou†[a], Ying Mei†[b,c], Yuhao Wang[a], Shenghua Zhou[b], Md Raziun Bin Mamtaz[a], Chuyang Y. Tang*[b], Francesco Ciucci*[a,d,e,f,g]

[a] Department of Mechanical and Aerospace Engineering, The Hong Kong University of Science and Technology, Clear Water Bay, Hong Kong SAR 999077, China

[b] Department of Civil Engineering, The University of Hong Kong, Pokfulam Road, Hong Kong SAR 999077, China

[c] Research and Development Center for Watershed Environmental Eco-Engineering, Advanced Institute of Natural Sciences, Beijing Normal University, Zhuhai 519000, China

[d] Department of Chemical and Biological Engineering, The Hong Kong University of Science and Technology, Clear Water Bay, Hong Kong SAR 999077, China

[e] HKUST Fok Ying Tung Research Institute, Guangzhou 510000, China

[f] HKUST Energy Institute, The Hong Kong University of Science and Technology, Clear Water Bay, Hong Kong SAR 999077, China

[g] HKUST Shenzhen-Hong Kong Collaborative Innovation Research Institute, Shenzhen 518000, China

*Correspondence: tangc@hku.hk

*Correspondence: francesco.ciucci@ust.hk

† G.Z. and Y.M. contributed equally to this work.

Experimental methods

Synthesis of NZSP and NZMSP

The NZSP was synthesized by a sol-gel method. First, a solution containing tetraethyl orthosilicate (TEOS), ethanol, and deionized water was prepared with a molar ratio of 1:10:20. Citric acid was then added to the solution under magnetic stirring at 60°C. Stoichiometric quantities of $NaNO_3$ and $ZrO(NO_3)_2$ were dissolved into deionized water and then added to the previous solution. 15% of extra $NaNO_3$ was added to compensate for Na evaporation during sintering. After that, an $(NH_4)_2HPO_4$ aqueous solution was added to form a collosol. The collosol was stirred at 80°C until a white gel was formed. Next, the gel was dried at 150°C before calcination at 900°C for 24 h. The resulting white powder was ball milled, pressed, and then sintered at 1150°C for 24 h. Finally, the sintered pellet was cracked and ball milled to obtain the NZSP powder. NZMSP was synthesized using the same method, except that 10% of the $ZrO(NO_3)_2$ was replaced by $Mg(NO_3)_2$.

Preparation of dense, porous, and bilayer pellets

Three types of pellets (dense, porous, and bilayer) were prepared in the current study. The dense pellets were prepared by a process involving cold pressing and sintering. The NZSP and NZMSP powders were uniaxially pressed into a disc with a diameter of 15 mm in a stainless-steel mold with a total load of 20 tons. The discs were then sintered at 1150°C for 5 h on a ZrO_2 plate. This sintering condition was used for all experiments unless otherwise specified. The prepared pellets were then reduced to desired thicknesses. The porous pellets were fabricated by mixing in a mortar the

NZSP/NZMSP powder with various ratios of corn starch. The obtained mixture was then pressed into a disc with a diameter of 15 mm in a stainless-steel mold under a total load of 10 tons. The discs were then sintered to obtain porous pellets. Two different methods were used to adjust the thickness of the dense part of the bilayer pellets. The first one was standard co-pressing. Specifically, the NZMSP powder was first spread on a stainless-steel mold. The NZMSP-corn starch mixture was then added above and co-pressed (20 tons) into a disc with a diameter of 15 mm. The obtained disc was finally sintered to realize a bilayer pellet. The second method, termed spray transfer, was used to prepare an ultrathin dense layer. 1 g of NZMSP was first ball-milled in 20 mL of ethanol for 24 h. Then, the obtained NZMSP/ethanol dispersion (1–4 mL) was sprayed on a polyethylene terephthalate (PET) sheet (3 × 5 cm) on a 200 ℃ hot plate. The PET sheet was then cut into discs with a diameter of 15 mm and placed on the bottom of the stainless-steel mold. NZMSP-corn starch mixture was added on top of the disc and uniaxially pressed into a pellet together under a total load of 20 tons. After that, the PET was peeled off from the pellet. The disc was finally sintered to obtain a bilayer pellet with an ultrathin dense layer.

Material characterization

XRD was performed on PANalytical Empyrean using Cu Kα radiation (λ = 1.5406 Å) in the 2θ range from 10 to 80° at an operation voltage of 40 kV and a current of 40 mA. The pellets' relative densities were measured using Archimedes' method. SEM was conducted using a JEOL-6390. EIS was carried out with an electrochemical workstation (VSP-300, BioLogic) to measure the ionic conductivities of NZSP/NZMSP. The

NZSP/NZMSP pellets used in the EIS tests were coated with gold paste and heated at 700°C for 1 h to form Na-blocking layers. Silver wires were then attached symmetrically before curing at 200°C for 4 h.

Membrane permselectivity tests

The permselectivity of an IEM is defined as the ability of the membrane to selectively allow the transport of counter-ions (*i.e.*, cations for CEMs and anions for AEMs) while hindering the transport of co-ions (*i.e.*, anions for CEMs and cations for AEMs). In this study, it was measured using a two-compartment cell comprising a HS (*e.g.*, 0.6 M NaCl) and a LS stream (*e.g.*, 0.02 M NaCl). Two Ag/AgCl reference electrodes were placed in each compartment for testing electrical diffusion potential over the membrane sample. The permselectivity (α) was calculated as the ratio of the experimental (E_{measured}) and theoretical ($E_{\text{theoretical}}$) potentials[1-3]:

$$\alpha = \frac{E_{\text{measured}}}{E_{\text{theoretical}}}$$

where $E_{\text{theoretical}} = \frac{\alpha RT}{zF} \ln\left(\frac{C_{\text{HS}}}{C_{\text{LS}}}\right)$ was obtained using Nernst equation. In the latter equation, α is the average membrane permselectivity of the ion exchange membranes, R is the universal gas constant (8.314 J mol^{-1} K^{-1}), T is the absolute temperature (296 K), z is the electrochemical valence, F is the Faraday constant (96485 C mol^{-1}), and C_{HS} and C_{LS} are the HS and LS salt concentrations (in mol L^{-1}), respectively.

RED tests

An RED stack with a single cell (*i.e.*, a pair of HS and LS compartments) was used to evaluate the power performance of the fabricated membranes. Specifically, the RED

stack comprised two poly(methyl methacrylate) chambers (each with an electrolyte volume of 20 mL) with a piece of membrane (effective area of 0.785 mm^2) mounted between the chambers. A pair of Ag/AgCl electrodes were used to apply a transmembrane potential and record the current output with an electrochemical working station (VSP-300, BioLogic) during the power performance measurement. The distance between the Ag/AgCl electrodes was kept at 10 mm. The presence of Ag/AgCl electrodes gave rise to additional redox potential, owing to the unequal liquid junction potentials of the electrodes in solutions with different concentrations. The redox potential of each electrode can be obtained by measuring its junction potential in the corresponding electrolyte versus a commercial Ag/AgCl reference electrode using a three electrodes system, following the method described by Jiang's group[4, 5]. Before each experiment, the Ag/AgCl reference electrodes were rechlorinated to ensure a constant potential. Therefore, the practical potential generated from the salinity gradient was corrected with the redox potential caused by the Ag/AgCl reference electrodes. NaCl solutions of 0.6 M and 0.02 M for power performance measurement were filled in the HS chamber and LS chamber, respectively. In addition, all the measurements were performed quickly and accomplished within 2 minutes to minimize the Ag/AgCl electrode potential variation under bias. Testing electrolytes were refreshed before each test. The area resistance, permselectivity, and power density presented in this work were averaged over four parallel tests as shown by the error bars. Commercial CEM CMV (Selemion, Japan) was also tested for comparison.

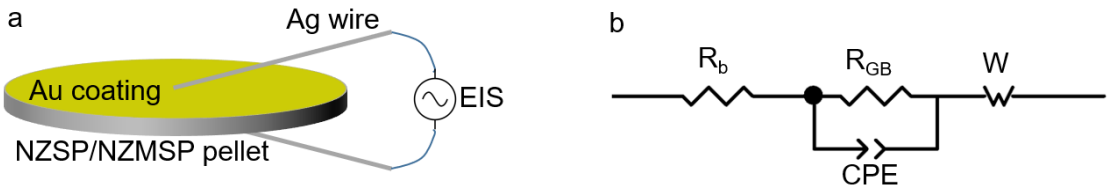

Figure S1. EIS test of NZSP/NZMSP. (a) Configuration of EIS test of the pellets. (b) Fitting model of the EIS curves.

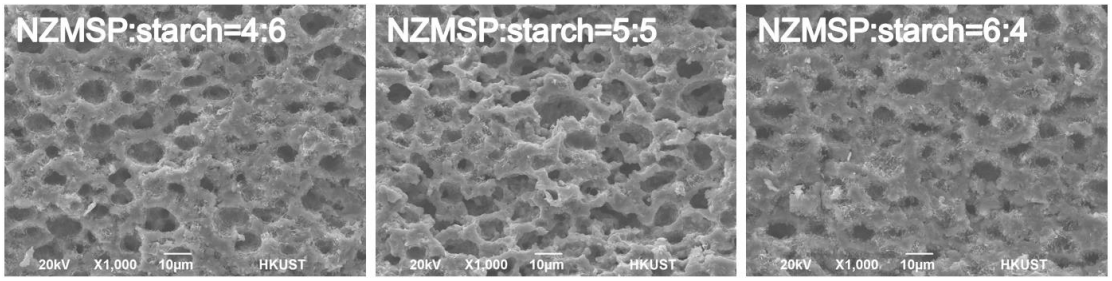

Figure S2. SEM images of porous NZMSP pellets prepared with various NZMSP-starch ratios.

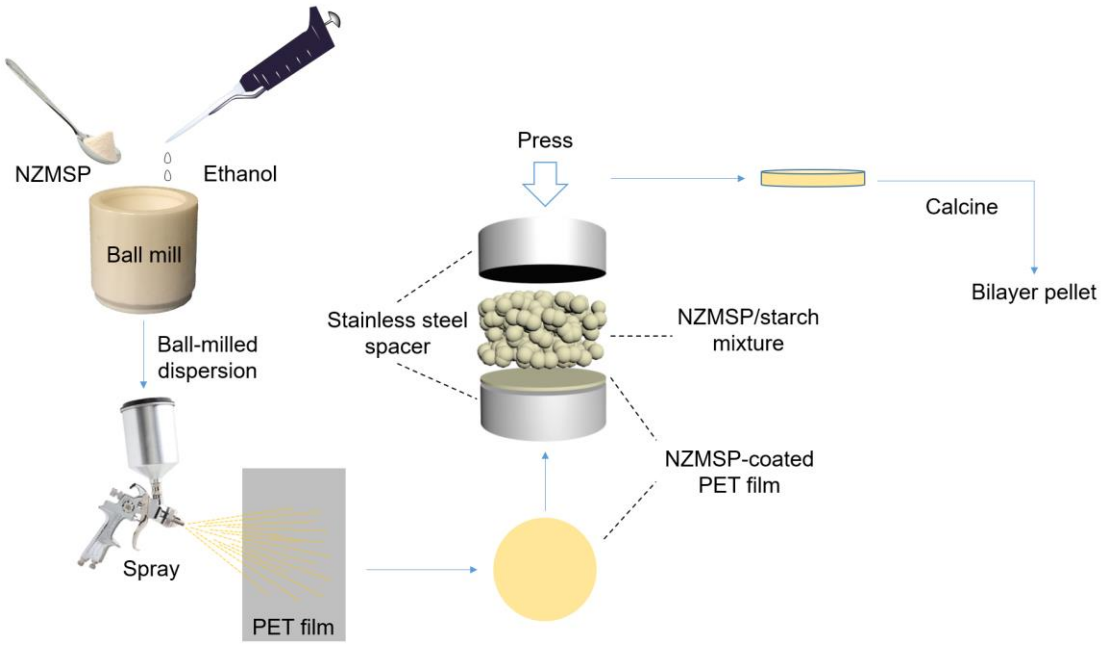

Figure S3. Schematic showing the preparation of bilayer pellets with the spray-transfer method.

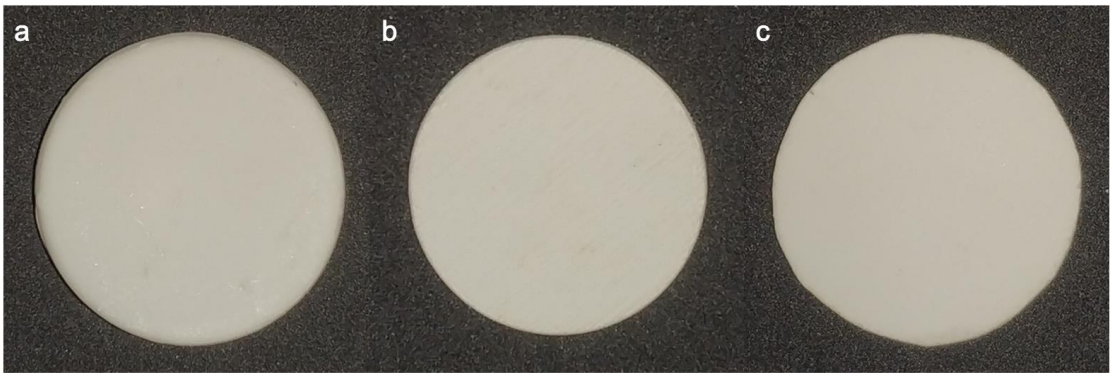

Figure S4. Optical photos of the dense, porous, and bilayer NZMSP membranes.

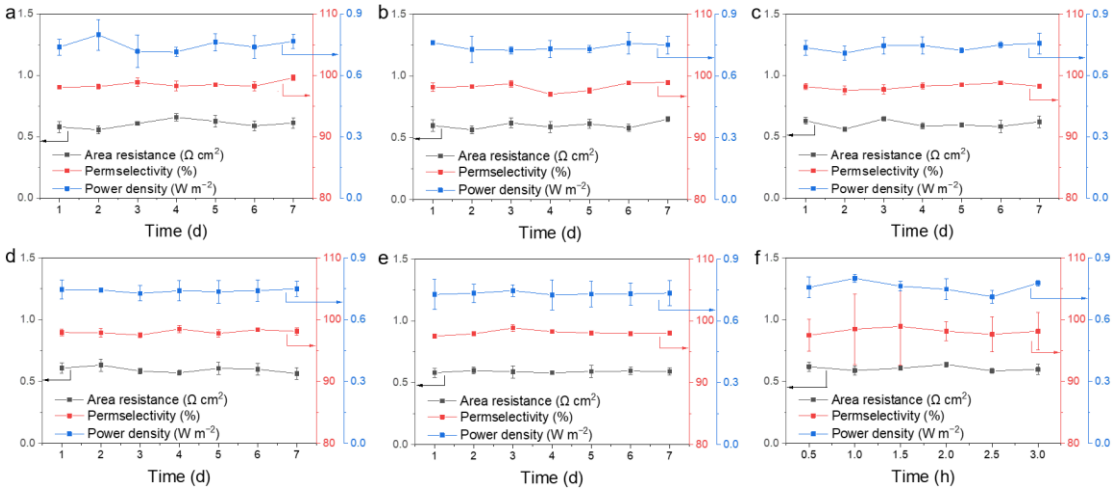

Figure S5. RED performance change of the NZMSP membrane after treatment with (a) 1 M NaCl, (b) 1 M $MgCl_2$, (c) 1 M NH_3, (d) 1 M NaOH, (e) 3 vol.% H_2O_2, and (f) UV light.

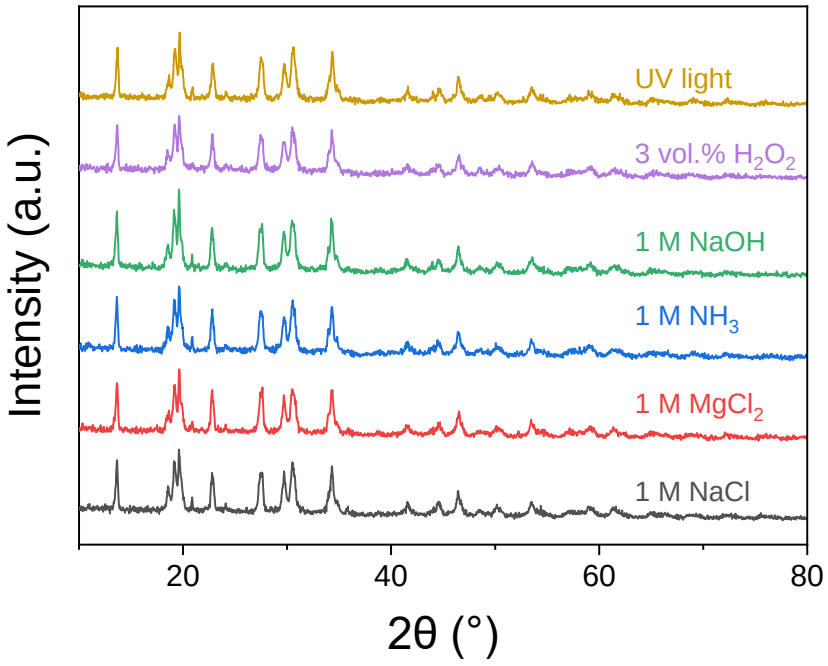

Figure S6. XRD patterns of the NZMSP after treatment with 1 M NaCl, 1 M $MgCl_2$, 1 M NH_3, 1 M NaOH, 3 vol.% H_2O_2, and UV light.

Table S1. Conductivities and sintering temperatures of doped NZSP obtained from the literature.

	Dopant	Doping level (at.%)	Sintering temperature (°C)	Bulk conductivity (mS cm^{-1})	Total conductivity (mS cm^{-1})	Reference
$Na_3Zr_2Si_2PO_{12}$			1200	2.0	0.67	[6, 7]
$Na_{3.4}Zr_{1.8}Mg_{0.2}Si_2PO_{12}$	Mg	10	1200	4.0	2.4	[8]
$Na_{3.1}Zr_{1.95}Mg_{0.05}Si_2PO_{12}$	Mg	2.5			3.5	[9]
$Na_{3.2}Zr_{1.9}Ca_{0.1}Si_2PO_{12}$	Ca	5	1250		1.67	[10]
$Na_{3.4}Zr_{1.6}Sc_{0.4}Si_2PO_{12}$	Sc	20	1265	6.2	4.0	[11]
$Na_{3.4}Zr_{1.6}Sc_{0.4}Si_2PO_{12}$	Sc	20	1260		2.0	[12]
$Na_{3.33}Zr_{1.67}Sc_{0.29}Yb_{0.04}Si_2PO_{12}$	Sc, Yb	14.5, 2.0	1250		1.62	[13]
$Na_{3.4}Zr_{1.8}Co_{0.2}Si_2PO_{12}$	Co	10	1125	3.33	1.55	[14]
$Na_3Zr_{1.8}Zn_{0.2}Si_2PO_{11.8}$	Zn	10	1225	3.41	1.44	[15]
$Na_{3.1}Zr_{1.9}La_{0.1}Si_2PO_{12}$	La	5	1150	1.43	1.10	[16]
$Na_{3.3}Zr_{1.7}La_{0.3}Si_2PO_{12}$	La	15	1200	4.5	3.4	[7]
$Na_{3.2}Zr_{1.9}Ce_{0.1}Si_2PO_{12}$	Ce	5	1100		0.9	[17]

Table S2. Comparison of the RED performance of the bilayer NZMSP membranes with literature reports.

Material	Permselectivity (%)	Area resistance (Ω cm^2)	Salinity gradient (M/M)	Power density (W m^{-2})	Reference
Sulfonated polyetheretherketone, -SO_3^{2-}	95.3 89.1	2.05 1.22	0.53/0.017	1–1.3 1.13–1.25	[18]
sPPO, -SO_3^{2-}	96.2	0.86	0.599/0.017	1.34	[19]
Fe_2O_3-SO_4^{2-} sPPO, -SO_3^{2-}	77.1–92.3	0.82–2.26	0.5/0.017	1.4	[20]
O-MCNTs- sPPO, -SO_3^{2-}	90–95.3	0.45–0.7	0.5/0.017	0.37–0.48	[21, 22]
SiO_2–SO_3H sPPO, -SO_3^{2-}	79.1–94	0.85–1.87	0.5/0.017	0.8–1.3	[23]
PVA-sPPO, -SO_3^{2-}	80–87	1.3–2.1	0.5/0.017	0.3–0.46	[24]
Fuji CEMT1-polypyrrole-chitosan	87–91	2.12–2.87	4/0.5	0.3-0.6	[25]
poly(arylene ether sulfone)-1-methyl-imidazolium	94.35–98.63	9	0.5/0.017	0.6	[26]
CMV	91	3.28	0.6/0.02	0.57	
Bilayer-1 mL	**93**	**0.21**	**0.6/0.02**	**0.70**	
Bilayer-2 mL	**98**	**0.59**	**0.6/0.02**	**0.74**	
Bilayer-3 mL	**100**	**0.84**	**0.6/0.02**	**0.69**	
Bilayer-4 mL	**100**	**1.08**	**0.6/0.02**	**0.66**	**This work**
Bilayer-2 mL	**98**	**0.59**	**1/0.02**	**0.89**	
Bilayer-2 mL	**98**	**0.59**	**2/0.02**	**1.11**	
Bilayer-2 mL	**98**	**0.59**	**3/0.02**	**1.23**	
Bilayer-2 mL	**98**	**0.59**	**5/0.02**	**1.44**	

References

(1) Tufa, R. A.; Pawlowski, S.; Veerman, J.; Bouzek, K.; Fontananova, E.; di Profio, G.; Velizarov, S.; Goulão Crespo, J.; Nijmeijer, K.; Curcio, E. Progress and Prospects in Reverse Electrodialysis for Salinity Gradient Energy Conversion and Storage. *Appl. Energy* **2018**, *225*, 290-331. DOI: https://doi.org/10.1016/j.apenergy.2018.04.111.

(2) Mei, Y.; Yao, Z.; Ji, L.; Toy, P. H.; Tang, C. Y. Effects of Hypochlorite Exposure on the Structure and Electrochemical Performance of Ion Exchange Membranes in Reverse Electrodialysis. *J. Membr. Sci.* **2018**, *549*, 295-305. DOI: https://doi.org/10.1016/j.memsci.2017.12.016.

(3) Hou, S.; Zhang, Q.; Zhang, Z.; Kong, X.; Lu, B.; Wen, L.; Jiang, L. Charged Porous Asymmetric Membrane for Enhancing Salinity Gradient Energy Conversion. *Nano Energy* **2021**, *79*, 105509. DOI: https://doi.org/10.1016/j.nanoen.2020.105509.

(4) Xin, W.; Zhang, Z.; Huang, X.; Hu, Y.; Zhou, T.; Zhu, C.; Kong, X.-Y.; Jiang, L.; Wen, L. High-Performance Silk-Based Hybrid Membranes Employed for Osmotic Energy Conversion. *Nat. Commun.* **2019**, *10* (1), 3876. DOI: 10.1038/s41467-019-11792-8.

(5) Guo, W.; Cao, L.; Xia, J.; Nie, F.-Q.; Ma, W.; Xue, J.; Song, Y.; Zhu, D.; Wang, Y.; Jiang, L. Energy Harvesting with Single-Ion-Selective Nanopores: A Concentration-Gradient-Driven Nanofluidic Power Source. *Adv. Funct. Mater.* **2010**, *20* (8), 1339-1344, https://doi.org/10.1002/adfm.200902312. DOI: https://doi.org/10.1002/adfm.200902312.

(6) Zhang, Z.; Zhang, Q.; Ren, C.; Luo, F.; Ma, Q.; Hu, Y.-S.; Zhou, Z.; Li, H.; Huang, X.; Chen, L. A Ceramic/Polymer Composite Solid Electrolyte for Sodium Batteries. *J. Mater. Chem. A* **2016**, *4* (41), 15823-15828, 10.1039/C6TA07590H. DOI: 10.1039/C6TA07590H.

(7) Zhang, Z.; Zhang, Q.; Shi, J.; Chu, Y. S.; Yu, X.; Xu, K.; Ge, M.; Yan, H.; Li, W.; Gu, L.; et al. A Self-Forming Composite Electrolyte for Solid-State Sodium Battery with Ultralong Cycle Life. *Adv. Energy Mater.* **2017**, *7* (4), 1601196. DOI: 10.1002/aenm.201601196.

(8) Zhang, Z.; Zou, Z.; Kaup, K.; Xiao, R.; Shi, S.; Avdeev, M.; Hu, Y.-S.; Wang, D.; He, B.; Li, H.; et al. Correlated Migration Invokes Higher Na^+-Ion Conductivity in NaSICON-Type Solid Electrolytes. *Adv. Energy Mater.* **2019**, *9* (42), 1902373. DOI: 10.1002/aenm.201902373.

(9) Song, S.; Duong, H. M.; Korsunsky, A. M.; Hu, N.; Lu, L. A Na^+ Superionic Conductor for Room-Temperature Sodium Batteries. *Sci. Rep.* **2016**, *6* (1), 32330. DOI: 10.1038/srep32330.

(10) Lu, Y.; Alonso, J. A.; Yi, Q.; Lu, L.; Wang, Z. L.; Sun, C. A High-Performance Monolithic Solid-State Sodium Battery with Ca^{2+} Doped $Na_3Zr_2Si_2PO_{12}$ Electrolyte. *Adv. Energy Mater.* **2019**, *9* (28), 1901205. DOI: 10.1002/aenm.201901205.

(11) Ma, Q.; Guin, M.; Naqash, S.; Tsai, C.-L.; Tietz, F.; Guillon, O. Scandium-Substituted $Na_3Zr_2(SiO_4)_2(PO_4)$ Prepared by a Solution-Assisted Solid-State Reaction

Method as Sodium-Ion Conductors. *Chem. Mater.* **2016**, *28* (13), 4821-4828. DOI: 10.1021/acs.chemmater.6b02059.

(12) Lunghammer, S.; Prutsch, D.; Breuer, S.; Rettenwander, D.; Hanzu, I.; Ma, Q.; Tietz, F.; Wilkening, H. M. R. Fast Na Ion Transport Triggered by Rapid Ion Exchange on Local Length Scales. *Sci. Rep.* **2018**, *8* (1), 11970. DOI: 10.1038/s41598-018-30478-7.

(13) Pal, S. K.; Saha, R.; Kumar, G. V.; Omar, S. Designing High Ionic Conducting NASICON-type $Na_3Zr_2Si_2PO_{12}$ Solid-Electrolytes for Na-Ion Batteries. *J. Phys. Chem. C* **2020**, *124* (17), 9161-9169. DOI: 10.1021/acs.jpcc.0c00543.

(14) Jolley, A. G.; Cohn, G.; Hitz, G. T.; Wachsman, E. D. Improving the Ionic Conductivity of NASICON Through Aliovalent Cation Substitution of $Na_3Zr_2Si_2PO_{12}$. *Ionics* **2015**, *21* (11), 3031-3038. DOI: 10.1007/s11581-015-1498-8.

(15) Chen, D.; Luo, F.; Zhou, W.; Zhu, D. Influence of Nb^{5+}, Ti^{4+}, Y^{3+} and Zn^{2+} Doped $Na_3Zr_2Si_2PO_{12}$ Solid Electrolyte on Its Conductivity. *J. Alloys Compd.* **2018**, *757*, 348-355. DOI: https://doi.org/10.1016/j.jallcom.2018.05.116.

(16) Ruan, Y.; Song, S.; Liu, J.; Liu, P.; Cheng, B.; Song, X.; Battaglia, V. Improved Structural Stability and Ionic Conductivity of $Na_3Zr_2Si_2PO_{12}$ Solid Electrolyte by Rare Earth Metal Substitutions. *Ceram. Int.* **2017**, *43* (10), 7810-7815. DOI: https://doi.org/10.1016/j.ceramint.2017.03.095.

(17) Liu, S.; Zhou, C.; Wang, Y.; Wang, W.; Pei, Y.; Kieffer, J.; Laine, R. M. Ce-Substituted Nanograin $Na_3Zr_2Si_2PO_{12}$ Prepared by LF-FSP as Sodium-Ion Conductors. *ACS Appl. Mater. Interfaces* **2020**, *12* (3), 3502-3509. DOI: 10.1021/acsami.9b11995.

(18) Güler, E.; Elizen, R.; Vermaas, D. A.; Saakes, M.; Nijmeijer, K. Performance-Determining Membrane Properties in Reverse Electrodialysis. *J. Membr. Sci.* **2013**, *446*, 266-276. DOI: https://doi.org/10.1016/j.memsci.2013.06.045.

(19) Lee, J.-Y.; Kim, J.-H.; Lee, J.-H.; Kim, S.; Moon, S.-H. Morphologically Aligned Cation-Exchange Membranes by a Pulsed Electric Field for Reverse Electrodialysis. *Environ. Sci. Technol.* **2015**, *49* (14), 8872-8877. DOI: 10.1021/acs.est.5b01151.

(20) Gi Hong, J.; Chen, Y. Evaluation of Electrochemical Properties and Reverse Electrodialysis Performance for Porous Cation Exchange Membranes with Sulfate-Functionalized Iron Oxide. *J. Membr. Sci.* **2015**, *473*, 210-217. DOI: https://doi.org/10.1016/j.memsci.2014.09.012.

(21) Zhang, B.; Hong, J. G.; Xie, S.; Xia, S.; Chen, Y. An Integrative Modeling and Experimental Study on the Ionic Resistance of Ion-Exchange Membranes. *J. Membr. Sci.* **2017**, *524*, 362-369. DOI: https://doi.org/10.1016/j.memsci.2016.11.050.

(22) Tong, X.; Zhang, B.; Chen, Y. Fouling Resistant Nanocomposite Cation Exchange Membrane with Enhanced Power Generation for Reverse Electrodialysis. *J. Membr. Sci.* **2016**, *516*, 162-171. DOI: https://doi.org/10.1016/j.memsci.2016.05.060.

(23) Gi Hong, J.; Glabman, S.; Chen, Y. Effect of Inorganic Filler Size on Electrochemical Performance of Nanocomposite Cation Exchange Membranes for Salinity Gradient Power Generation. *J. Membr. Sci.* **2015**, *482*, 33-41. DOI:

https://doi.org/10.1016/j.memsci.2015.02.018.

(24) Zhang, H.; Jiang, D.; Zhang, B.; Hong, J. G.; Chen, Y. A Novel Hybrid Poly (vinyl alcohol) (PVA)/Poly (2,6-dimethyl-1,4-phenylene oxide) (PPO) Membranes for Reverse Electrodialysis Power System. *Electrochim. Acta* **2017**, *239*, 65-73. DOI: https://doi.org/10.1016/j.electacta.2017.04.008.

(25) Tufa, R. A.; Piallat, T.; Hnát, J.; Fontananova, E.; Paidar, M.; Chanda, D.; Curcio, E.; di Profio, G.; Bouzek, K. Salinity Gradient Power Reverse Electrodialysis: Cation Exchange Membrane Design Based on Polypyrrole-Chitosan Composites for Enhanced Monovalent Selectivity. *Chem. Eng. J.* **2020**, *380*, 122461. DOI: https://doi.org/10.1016/j.cej.2019.122461.

(26) Cho, D. H.; Lee, K. H.; Kim, Y. M.; Park, S. H.; Lee, W. H.; Lee, S. M.; Lee, Y. M. Effect Of Cationic Groups in Poly(Arylene Ether Sulfone) Membranes on Reverse Electrodialysis Performance. *Chem. Commun.* **2017**, *53* (15), 2323-2326, 10.1039/C6CC08440K. DOI: 10.1039/C6CC08440K.